COLOR SHRINKAGE FOR SPARSE CODING OF COLOR IMAGES

Takahiro Saito, Yasutaka Ueda, and Takashi Komatsu

Department of Electronics & Informatics Frontiers, Kanagawa University
3-27-1 Rokkakubashi, Kanagawa-ku, 221-8686, Yokohama, Japan
phone: + (81) 45 481 5661, fax: + (81) 45 491 7915, email: saitot01@kanagawa-u.ac.jp
web: http://slat4.ee.kanagawa-u.ac.jp

ABSTRACT

As a basic tool for deriving sparse representation of a color image from its atomic-decomposition with a redundant dictionary, this paper presents a new kind of shrinkage, viz. color shrinkage, which utilizes inter-channel color cross-correlations directly in the three primary color space. Among various schemes of color shrinkage, this paper particularly addresses the hard color-shrinkage, a natural extension of the classic hard-shrinkage, and shows the advantages over the existing shrinkage approach where the classic hard-shrinkage is applied after a non-redundant color transformation. Moreover, to mitigate defects of the existing shrinkage approach, this paper presents a new simple color-shrinkage scheme that applies the classic hard-shrinkage together with a redundant color transformation instead of a non-redundant color transformation. Furthermore, this paper applies our color-shrinkage schemes to color-image denoising in the tight-frame Haar wavelet transform domain, and experimentally demonstrates their superiority over the existing shrinkage approach.

1. INTRODUCTION

The sparse image-coding with a redundant dictionary, e.g. a frame, yields useful image-representation, by which efficient image restoration such as image denoising and image deblurring is successfully achieved [1]. Moreover, recently, in the field of the neuroscience, the working hypothesis that in a brain sensory signals are compactly represented by the sparse coding has rapidly been gaining ground [2]. The classic shrinkage methods such as the hard shrinkage and the soft shrinkage are basic tools by which sparse representation of a scalar image is derived from redundant atomic-decomposition of the image. Although the classic shrinkage methods are very simple, they efficiently yield desirable sparse-representation of a scalar image. However, since for a vector-valued image such as a primary color image, there are intensive inter-channel color cross-correlations, the classic shrinkage methods do not necessarily provide its desirable sparse-representation.

As a basic tool with which desirable sparse-representation of a primary color image is produced, the authors have been devising a new kind of shrinkage, named color shrinkage, that utilizes inter-channel color cross-correlations directly in the three primary color space [3], [4], [5]. This paper particularly addresses a new color-shrinkage scheme named hard color-shrinkage, which is a natural extension of the classic hard-shrinkage, and shows its superiority over the existing shrinkage approach that applies the classic hard-shrinkage together with a non-redundant color transformation such as the opponent color transformation. Moreover, to remedy drawbacks of the existing shrinkage approach, this paper presents a new simple color-shrinkage scheme that uses the classic hard-shrinkage together with a redundant color transformation instead of a non-redundant color transformation. Furthermore, this paper applies our color-shrinkage schemes to color-image denoising in the tight-frame Haar wavelet transform domain, and experimentally demonstrates their superiority over the existing shrinkage approach.

2. SPARSE CODING AND HARD SHRINKAGE

Let $\mathbf{d}_i$ a dictionary atom with unit l^2 norm defined in the N-dimensional space $\mathbf{R}^N$, and let the total number M of the dictionary atoms much larger than N. A dictionary matrix $\mathbf{D}$ is defined by arranging the M dictionary atoms, $\mathbf{d}_1, \mathbf{d}_2, \cdots, \mathbf{d}_M$, into a horizontally-long matrix form. Let the dictionary matrix $\mathbf{D}$ a full-rank matrix, i.e. Rank $(\mathbf{D}) = N$. On the above assumption, the problem of representing a scalar image $\mathbf{x} \in \mathrm{R}^N$ as a linear combination of the redundant dictionary atoms $\{\mathbf{d}_i\}$ is formulated as an under-determined linear simultaneous equation:

$$\mathbf{D} \cdot \boldsymbol{\varphi} = \mathbf{x}\,. \tag{1}$$

Given $\mathbf{x}$, its coefficient vector $\boldsymbol{\varphi}$ necessarily exists, but it is not uniquely determined. The best coefficient vector $\boldsymbol{\varphi}^{\mathrm{opt}}$ should be selected from the linear manifold $\mathbf{S}\,(\mathbf{D}, \mathbf{x})$ of solution vectors of the equation $\mathbf{D}\boldsymbol{\varphi} = \mathbf{x}$. If the dictionary $\mathbf{D}$ is proper for representing meaningful image features, those features will be almost completely represented as a linear combination of a few dictionary atoms; whereas visually meaningless entities such as noise cannot be accurately represented with a few dictionary atoms. Therefore, the linear combination of the fewest dictionary atoms will give the most appropriate coefficient vector $\boldsymbol{\varphi}^{\mathrm{opt}}$, and the problem of seeking for this solution is referred to as the sparse image-coding problem, which is formulated as the well-known matching-pursuit (MP) optimization problem of minimizing the l^0 norm of $\boldsymbol{\varphi}$ subject to $\mathbf{D}\boldsymbol{\varphi} = \mathbf{x}$. However, in most cases, the image $\mathbf{x}$ is contaminated with noise, and we should make allowance for representation errors; the sparse image-coding problem is usually formulated as the MP approximation (MPA) problem [1]:

$$\boldsymbol{\varphi}^{\mathrm{opt}} := \arg\min_{\boldsymbol{\varphi}} \left\|\mathbf{D} \cdot \boldsymbol{\varphi} - \mathbf{x}\right\|_2^2, \quad \text{subject to } \left\|\boldsymbol{\varphi}\right\|_0 \le R\,. \tag{2}$$

The MPA problem of (2) is an NP-complete problem, is not a convex optimization problem, and hence is hard to solve. However, its sub-optimal solvers have been proposed. Among them, the alternate-projection (AP) solver [6] is the most basic. The AP solver alternately iterates the two projections: 1) the orthogonal projection $\mathbf{P}_{\mathbf{S}\,(\mathbf{D},\,\mathbf{x})}\,(\boldsymbol{\varphi})$ of $\boldsymbol{\varphi}$ onto the linear manifold $\mathbf{S}\,(\mathbf{D}, \mathbf{x})$, and 2) the projection $\mathbf{P}_{L0(R)}\,(\boldsymbol{\varphi})$ of $\boldsymbol{\varphi}$ onto the l^0 ball $L^0\,(R)$: $= \{\boldsymbol{\varphi} \mid \|\boldsymbol{\varphi}\|_0 \le R\}$ with a radius R. The projection $\mathbf{P}_{L0(R)}\,(\boldsymbol{\varphi})$ is easily computed by selecting, from among the M elements of $\boldsymbol{\varphi}$, R elements with large magnitude in the magnitude-decreasing order and keeping them unchanged, and by annihilating the other elements to be null simultaneously. This amounts to applying the classic hard-shrinkage to the M elements of $\boldsymbol{\varphi}$. Let $\{\phi_1, \phi_2, \cdots, \phi_M\}$ the sequence of M elements of $\boldsymbol{\varphi}$ lined up in the magnitude-decreasing order, a threshold parameter μ of the hard shrinkage will be determined as a value satisfying the inequality $|\phi_{R+1}| \le \mu < |\phi_R|$, and thus the projection $\mathbf{P}_{L0(R)}\,(\boldsymbol{\varphi})$ will amount to applying the hard shrinkage HT with the threshold pa-

rameter μ to the M elements, $\varphi_1, \varphi_2, \cdots, \varphi_M$, of $\boldsymbol{\varphi}$, as follows:

$$\mathrm{HT}(\varphi_i;\mu) := \begin{cases} \varphi_i & , \ if \ |\varphi_i| > \mu, \\ 0 & , \ if \ |\varphi_i| \le \mu. \end{cases} \tag{3}$$

However, the projection $\mathbf{P}_{L0(R)}(\boldsymbol{\varphi})$ is not necessarily unique, because of the non-convexity of the l^0 ball $L^0(R)$. If $|\phi_{R+1}| = |\phi_R|$, then the projection will not be uniquely determined.

3. FROM SHRINKAGE TO COLOR SHRINKAGE

The classic shrinkage methods such as the hard shrinkage are derived as a solution of the optimization problem:

$$\hat{x} := \arg\min_x \mathrm{F}(x), \quad \mathrm{F}(x) := \left\{ |x|^p + \frac{\lambda}{2} \cdot |x - x_o|^2 \right\} \tag{4}$$
$$, \ \lambda > 0 \ ; \ x_o : \text{Input}, \ x : \text{Output}.$$

If the parameter p in (4) is set to $p = 0$, $p = 1$ and $p = 2$, then the optimal solution of (4) will be the hard shrinkage HT (x; $(2/\lambda)^{1/2}$), the soft shrinkage ST (x; $1/\lambda$) and the linear shrinkage LS (x; λ), respectively. The linear shrinkage LS (x; λ) is defined by

$$\mathrm{LS}(x;\lambda) := \lambda \cdot x / (2 + \lambda), \tag{5}$$

but it is not useful for the sparse coding of a scalar image.

To utilize interdependence among the three primary color channels for the shrinkage, we introduce into (4) the l^p norms of color differences and the l^p norms of color sums among atomic-decomposition coefficients of the three primary color signals, and thus we formulate the optimization problem [3], [4], [5]:

$$\hat{\mathbf{p}} := \min_{\mathbf{p}} \mathrm{E}(\mathbf{p}), \qquad \mathbf{p} := (r, g, b)^{\mathrm{T}} \tag{6}$$

$$\begin{aligned} \mathrm{E}(\mathbf{p}) := & |r|^p + |g|^p + |b|^p + \alpha \cdot |r - g|^p + \beta \cdot |r + g|^p \\ & + \alpha \cdot |g - b|^p + \beta \cdot |g + b|^p + \alpha \cdot |b - r|^p + \beta \cdot |b + r|^p \\ & + \lambda_R \cdot (r - r_o)^2 / 2 + \lambda_G \cdot (g - g_o)^2 / 2 + \lambda_B \cdot (b - b_o)^2 / 2 \end{aligned}$$

where $\mathbf{p}_o = (r_o, g_o, b_o)^{\mathrm{T}}$ is an input color vector and $\mathbf{p} = (r, g, b)^{\mathrm{T}}$ is an output color vector. The five parameters, α, β, and λ_p ($p = R, G, B$), are set to satisfy $\alpha \ge 0$, $\beta \ge 0$, and $\lambda_p > 0$ ($p = R, G, B$).

In (6), the l^0 norms of the three components of $\mathbf{p}$ operate to suppress their irregular variations caused by additive noise. The l^0 norms of color differences such as $r - g$ operate to preserve identically-varying variations in which the two color signals change in phase with each other; whereas the l^0 norms of color sums such as $r + g$ operate to preserve oppositely-varying variations in which one color signal increases while the other color signal decreases [7]. For most of natural color images, the occurrence probability of the identically-varying variations is considered higher than that of the oppositely-varying variations, and hence the two parameters, α, β, are usually set so that the inequality $\alpha > \beta$ may be satisfied. The last three terms of l^2 norms in (6) are the data-fidelity terms, and the three parameters, λ_R, λ_G, λ_B, are referred to as the shrinkage parameters.

Three different color-shrinkage methods are derived as a solution of the optimization problem of (6) [3], [4], [5].

1) Hard color-shrinkage: It is natural extension of the hard shrinkage, and is an optimal solution in the case of $p = 0$. The hard color-shrinkage is constructed as a non-iterative algorithm that computes the energy values of E for all of its finite feasible solutions and then chooses one feasible solution giving the minimum energy value.

2) Soft color-shrinkage [3], [4]: It is natural extension of the soft shrinkage, and is an optimal solution in the case of $p = 1$. The soft color shrinkage is constructed as an iterative algorithm.

3) Linear color-shrinkage [5]: It is natural extension of the linear shrinkage, and is an optimal solution in the case of $p = 2$. The linear color shrinkage is constructed as a solution of a linear simultaneous equation with three unknowns, r, g, b, but is not useful for the sparse coding of a color image. If the three shrinkage parameters are set equal to each other, i.e. $\lambda_R = \lambda_G = \lambda_B$, then the linear color-shrinkage will amount to applying the classic linear-shrinkage separately to each color component in the opponent color space.

4. HARD COLOR-SHRINKAGE

If the parameter p is set to 0 in (6), then the energy function E ($\mathbf{p}$) will not be convex with respect to $\mathbf{p}$ and its optimal solution will not uniquely determined. However, one of its optimal solutions is easily sought in the manner described below.

The energy function E ($\mathbf{p}$) in (6) has the following nine plane crevices passing through the origin (0, 0, 0):

$$\{r = 0, g = 0, b = 0, r = g, g = b, b = r, r = -g, g = -b, b = -r\}. \tag{7}$$

On the nine plane crevices, E ($\mathbf{p}$) appears as different bi-variable quadratic polynomial functions. On each plane crevice, the optimization problem of (6) can be converted into a two-variable optimization problem with the canonical form:

$$\min_{x,y} \mathrm{G}(x, y), \tag{8}$$

$$\begin{aligned} \mathrm{G}(x,y) := & |x|^0 + \gamma' |y|^0 + \alpha' |x - y|^0 + \beta' |x + y|^0 \\ & + \lambda_X (x - x_o)^2 / 2 + \lambda_Y (y - y_o)^2 / 2 \\ & ; \ \alpha' \ge 0, \ \beta' \ge 0, \ \gamma' > 0, \ \lambda_X > 0, \ \lambda_Y > 0, \end{aligned}$$

where (x_o, y_o) are inputs and (x, y) are outputs. The five parameters, α', β', γ', λ_X, λ_Y, are uniquely determined from the original five parameters α, β, λ_R, λ_G, λ_B.

The energy function G (x, y) in (8) has the following four linear crevices passing through the origin (0, 0):

$$\{x = 0, \ y = 0, \ x = y, \ x = -y\}. \tag{9}$$

On the four linear crevices, the energy function G (x, y) appears as different single-variable quadratic polynomial functions. The origin (0, 0) is a singular point common to all the linear crevices. From these properties, we can enumerate all six feasible solutions of (8), as follows.

0) Origin (0, 0): The origin is a feasible solution common to all the four linear crevices.

1) Feasible solution in a 2-D region except the four linear crevices: This corresponds to the case of $\{x \ne 0, y \ne 0, x \ne y, x \ne -y\}$. In this case, the energy function G (x, y) has its minimum at (x, y) = (x_o, y_o), and its feasible solution is (x_o, y_o).

2) Feasible solution, except the origin (0, 0), on the linear crevice $x = 0$: This corresponds to the case of $\{x = 0, y \ne 0\}$, and its feasible solution is (0, y_o).

3) Feasible solution, except the origin (0, 0), on the linear crevice $y = 0$: This corresponds to the case of $\{x \ne 0, y = 0\}$, and its feasible solution is (x_o, 0).

4) Feasible solution, except the origin (0, 0), on the linear crevice $x = y$: This corresponds to the case of $\{x = y = t, t \ne 0\}$. In this case, the energy function G (t, t) has its minimum at

$$t = s_4 := (\lambda_X x_o + \lambda_Y y_o) / (\lambda_X + \lambda_Y), \tag{10}$$

and its feasible solution is (s_4, s_4).

5) Feasible solution, except the origin (0, 0), on the linear crevice $x = -y$: This corresponds to the case of $\{x = -y = t, t \ne 0\}$. In this case, the energy function G (t, $-t$) has its minimum at

$$t = s_5 := (\lambda_X x_o - \lambda_Y y_o) / (\lambda_X + \lambda_Y), \tag{11}$$

and its feasible solution is (s_5, $-s_5$).

Each feasible solution of (8) occupies its territory in the 2-D space of the two input variables, x_o, y_o. In Fig. 1, in the two cases of typical setting of the five parameters, α', β', γ', λ_X, λ_Y, in (8), we show the territories of the six feasible solutions: {(0, 0), (x_o, y_o), (0, y_o), (x_o, 0), (s_4, s_4), (s_5, $-s_5$)}. Figure 1(a) corresponds to the case of

$\{\alpha' = 0, \beta' = 0, \gamma' = 1\}$, in which inter-variable cross-correlations are not utilized, and hence only the four feasible solutions, $\{(0, 0), (x_o, y_o), (0, y_o), (x_o, 0)\}$, have their territories in the 2-D space, and the territories coincide with those of the classic hard-shrinkage, i.e. in this parameter setting the hard color-shrinkage amounts to the classic hard-shrinkage. Figure 1(b) corresponds to the case of $\{\alpha' = 5, \beta' = 1, \gamma' = 1\}$, where inter-variable cross-correlations are utilized, and the territories of the six feasible solutions have their respective complex shapes, especially near the origin (0, 0), and their shapes depend on the setting of the five parameters, α', β', γ', λ_X, λ_Y.

On each plane crevice of $\mathrm{E}(\mathbf{p})$ in (6), there exists six feasible solutions, but a certain feasible solution may coincide with other feasible solutions. There necessarily exists a straight line common to two different plane crevices, the line coincides with one of the linear crevices, and on the linear crevice there necessarily exists feasible solutions common to the two plane crevices. In addition, the origin (0, 0, 0) is a feasible solution common to all the nine plane crevices. Listing all feasible solutions without duplication, we have 24 feasible solutions in all, and we denote them by $\{\mathbf{c}^{(k)} := (r^{(k)}, g^{(k)}, b^{(k)}); k = 0, \cdots, 23\}$. Table 1 shows all the feasible solutions. When we exclude the three l^0-norm terms of color sums from $\mathrm{E}(\mathbf{p})$ in (6) by setting β to 0, its feasible solutions is limited to the subset composed of fifteen feasible solutions, viz. $\{\mathbf{c}^{(k)}; k = 0,\cdots, 8$, and $k = 12,\cdots, 17\}$.

The shape of the territory occupied by each feasible solution is complex, and depends on the setting of the five parameters. Hence, a computational algorithm of seeking for the optimal solution is not constructed as a series of simple-thresholding operations. Instead, the hard color-shrinkage is constructed as the following computational algorithm.

[Computational Algorithm of the Hard Color-Shrinkage]

1) For each feasible solution $\mathbf{c}^{(k)}$, firstly we compute its energy value $E^{(k)} := \mathrm{E}(\mathbf{c}^{(k)})$.
2) As the optimal solution, we select a feasible solution giving the minimum energy value from among the 24 feasible solutions:

$$\hat{\mathbf{p}} := \arg \min_{\{\mathbf{c}^{(k)} \mid k=0,1,\cdots,23\}} \mathrm{E}(\mathbf{c}^{(k)}). \tag{12}$$

3) If there are plural feasible solutions giving the minimum energy value, from among them we will select one feasible solution with the fewest nonzero components. This rule is proper for the sparse representation of color images. [End of the Algorithm]

5. HARD SHRINKAGE IN THE ORTHOGONAL OPPONENT COLOR SPACE

The classic approach to the utilization of inter-channel color cross-correlations for the shrinkage of atomic-decomposition coefficients of a color image is to apply the classic shrinkage such as the hard shrinkage after the non-redundant color transformation of the atomic-decomposition coefficients. As the non-redundant color transformation, this paper takes up the well-known opponent color transformation, which is a kind of orthogonal color transformation. The orthogonal opponent color transformation is defined by

$$\begin{pmatrix} o_1 \\ o_2 \\ o_3 \end{pmatrix} = \begin{pmatrix} 1 & 1 & 1 \\ 1 & 0 & -1 \\ 1 & -2 & 1 \end{pmatrix} \cdot \begin{pmatrix} r \\ g \\ b \end{pmatrix} \tag{13}$$

Similarly in the case of the hard color-shrinkage, we can easily enumerate all feasible solutions of the classic hard-shrinkage in the orthogonal opponent color space, in the following manner. By firstly applying the hard shrinkage separately to the three components of the orthogonal opponent color vector $\mathbf{o} = (o_1, o_2, o_3)^{\mathrm{T}}$ and then transforming the shrunken color vector into the three primary color vector, all feasible solutions in the RGB primary color space are enumerated. The hard shrinkage in the orthogonal opponent color space has its eight feasible solutions, $\{\mathbf{d}^{(k)} := (r^{(k)}, g^{(k)}, b^{(k)}); k = 0, \cdots, 7\}$, which are shown in Table 2.

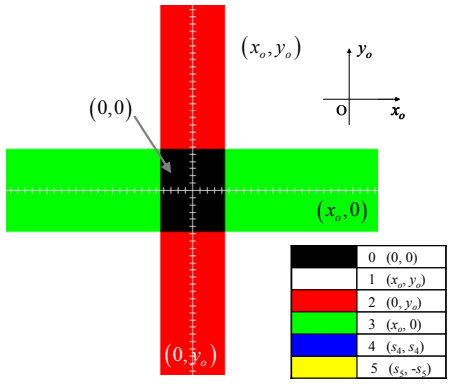

(a) $\alpha' = 0, \beta' = 0, \gamma' = 1, \lambda_X = 0.0005, \lambda_Y = 0.0003$

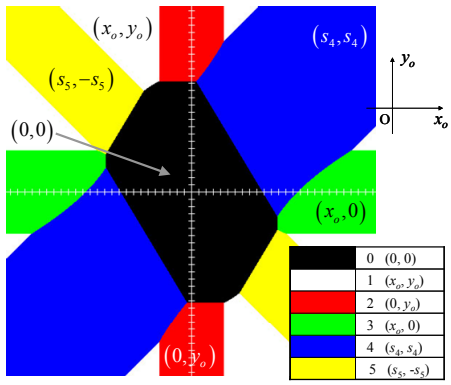

(b) $\alpha' = 5, \beta' = 1, \gamma' = 1, \lambda_X = 0.0005, \lambda_Y = 0.0003$

Figure 1 – Territories of the six feasible solutions, (0, 0), (x_o, y_o), $(0, y_o)$, $(x_o, 0)$, (s_4, s_4), $(s_5, -s_5)$, of the canonical two-variable optimization problem of (9).

Table 1 – 24 feasible solutions $\{\mathbf{c}^{(k)} := (r^{(k)}, g^{(k)}, b^{(k)}); k = 0, 1, \cdots, 23\}$ of the hard color-shrinkage.

$\mathbf{c}^{(0)} = (0, 0, 0)$; $\mathbf{c}^{(1)} = (r_o, g_o, b_o)$
$\mathbf{c}^{(2)} = (r_o, g_o, 0)$; $\mathbf{c}^{(3)} = (0, g_o, b_o)$; $\mathbf{c}^{(4)} = (r_o, 0, b_o)$
$\mathbf{c}^{(5)} = (r_o, 0, 0)$; $\mathbf{c}^{(6)} = (0, g_o, 0)$; $\mathbf{c}^{(7)} = (0, 0, b_o)$
$\mathbf{c}^{(8)} = (t_8, t_8, t_8)$, $t_8 = (\lambda_R r_o + \lambda_G g_o + \lambda_B b_o)/(\lambda_R + \lambda_G + \lambda_B)$
$\mathbf{c}^{(9)} = (t_9, -t_9, -t_9)$, $t_9 = (\lambda_R r_o - \lambda_G g_o - \lambda_B b_o)/(\lambda_R + \lambda_G + \lambda_B)$
$\mathbf{c}^{(10)} = (-t_{10}, t_{10}, -t_{10})$, $t_{10} = (-\lambda_R r_o + \lambda_G g_o - \lambda_B b_o)/(\lambda_R + \lambda_G + \lambda_B)$
$\mathbf{c}^{(11)} = (-t_{11}, -t_{11}, t_{11})$, $t_{11} = (-\lambda_R r_o - \lambda_G g_o + \lambda_B b_o)/(\lambda_R + \lambda_G + \lambda_B)$
$\mathbf{c}^{(12)} = (t_{12}, t_{12}, 0)$; $\mathbf{c}^{(13)} = (t_{12}, t_{12}, b_o)$, $t_{12} = (\lambda_R r_o + \lambda_G g_o)/(\lambda_R + \lambda_G)$
$\mathbf{c}^{(14)} = (0, t_{14}, t_{14})$; $\mathbf{c}^{(15)} = (r_o, t_{14}, t_{14})$, $t_{14} = (\lambda_G g_o + \lambda_B b_o)/(\lambda_G + \lambda_B)$
$\mathbf{c}^{(16)} = (t_{16}, 0, t_{16})$; $\mathbf{c}^{(17)} = (t_{16}, g_o, t_{16})$, $t_{16} = (\lambda_B b_o + \lambda_R r_o)/(\lambda_B + \lambda_R)$
$\mathbf{c}^{(18)} = (t_{18}, -t_{18}, 0)$; $\mathbf{c}^{(19)} = (t_{18}, -t_{18}, b_o)$; $t_{18} = (\lambda_R r_o - \lambda_G g_o)/(\lambda_R + \lambda_G)$
$\mathbf{c}^{(20)} = (0, t_{20}, -t_{20})$; $\mathbf{c}^{(21)} = (r_o, t_{20}, -t_{20})$; $t_{20} = (\lambda_G g_o - \lambda_B b_o)/(\lambda_G + \lambda_B)$
$\mathbf{c}^{(22)} = (-t_{22}, 0, t_{22})$; $\mathbf{c}^{(23)} = (-t_{22}, g_o, t_{22})$; $t_{22} = (\lambda_B b_o - \lambda_R r_o)/(\lambda_B + \lambda_R)$

In comparison with the feasible-solution set $\{\mathbf{c}^{(k)}\}$ of the hard color-shrinkage, the feasible-solution set $\{\mathbf{d}^{(k)}\}$ in Table 2 lacks symmetry and balance in its structure. As shown in Table 1, the feasible-solution set $\{\mathbf{c}^{(k)}\}$ has the three feasible solutions that render one output primary color value equal with its corresponding

input color value and simultaneously force the other two output primary color values to be equal with each other. On the other hand, as shown in Table 2, the feasible-solution set $\{\mathbf{d}^{(k)}\}$ has only one feasible solution having such a property. If the hard shrinkage in the orthogonal opponent color space is applied to color-image denoising, false color artifacts will be caused by this asymmetry and imbalance.

Table 2 – Eight feasible solutions $\{\mathbf{d}^{(k)}: = (r^{(k)}, g^{(k)}, b^{(k)}); k = 0, 1, \cdots, 7\}$ of the hard shrinkage in the orthogonal opponent color space.

$\mathbf{d}^{(0)} = (0,0,0)$; $\mathbf{d}^{(1)} = (r_o, g_o, b_o)$
$\mathbf{d}^{(2)} = (t,t,t)$, $t = (r_o + g_o + b_o)/3$
$\mathbf{d}^{(3)} = \left(\frac{2r_o - g_o - b_o}{3}, \frac{-r_o + 2g_o - b_o}{3}, \frac{-r_o - g_o + 2b_o}{3}\right)$
$\mathbf{d}^{(4)} = \left(\frac{r_o + b_o}{2}, g_o, \frac{r_o + b_o}{2}\right)$
$\mathbf{d}^{(5)} = \left(\frac{r_o - b_o}{2}, 0, \frac{-r_o + b_o}{2}\right)$
$\mathbf{d}^{(6)} = \left(\frac{5r_o + 2g_o - b_o}{6}, \frac{r_o + g_o + b_o}{3}, \frac{-r_o + 2g_o + 5b_o}{6}\right)$
$\mathbf{d}^{(7)} = \left(\frac{r_o - 2g_o + b_o}{6}, \frac{-r_o + 2g_o - b_o}{3}, \frac{r_o - 2g_o + b_o}{6}\right)$

6. HARD SHRINKAGE IN THE REDUNDANT COLOR SPACE

To remedy the asymmetry and the imbalance of the feasible-solution set of the hard shrinkage in the orthogonal opponent color space, this paper introduces a new color-shrinkage approach with redundant color transformation. By modifying the orthogonal opponent color transformation of (13), this paper constructs new redundant color transformation with symmetry about the three primary colors, (r, g, b), which is defined by

$$\begin{pmatrix} q_1 \\ q_2 \\ q_3 \\ q_4 \end{pmatrix} = \begin{pmatrix} 1 & 1 & 1 \\ 1 & -1 & 0 \\ 0 & 1 & -1 \\ -1 & 0 & 1 \end{pmatrix} \cdot \begin{pmatrix} r \\ g \\ b \end{pmatrix} \tag{14}$$

Its left inverse color transformation, i.e. the least squares generalized inverse transformation, is given by

$$\begin{pmatrix} r \\ g \\ b \end{pmatrix} = \frac{1}{3} \cdot \begin{pmatrix} 1 & 1 & 0 & -1 \\ 1 & -1 & 1 & 0 \\ 1 & 0 & -1 & 1 \end{pmatrix} \cdot \begin{pmatrix} q_1 \\ q_2 \\ q_3 \\ q_4 \end{pmatrix} \tag{15}$$

Similarly in the case of the hard shrinkage with the orthogonal opponent color transformation, we can easily enumerate all feasible solutions of the new color-shrinkage approach that apply the hard-shrinkage separately to the four redundant components of the color vector $\mathbf{q} = (q_1, q_2, q_3, q_4)^{\mathrm{T}}$. The hard shrinkage in the redundant color space of $\mathbf{q}$ has sixteen feasible solutions, $\{\mathbf{e}^{(k)}: = (r^{(k)}, g^{(k)}, b^{(k)}); k = 0, \cdots, 15\}$, which are shown in Table 3.

As shown in Table 3, the feasible-solution set $\{\mathbf{e}^{(k)}\}$ is symmetric and well-balanced, but in trade-off between symmetry and compactness the feasible-solution set $\{\mathbf{e}^{(k)}\}$ may be somewhat inferior to the feasible-solution set $\{\mathbf{c}^{(k)}\}$ of our hard color-shrinkage. The hard shrinkage in the redundant color space is expected to achieve shrinkage performance intermediate between our hard color-shrinkage and the existing hard-shrinkage approach with the orthogonal opponent color transformation.

Table 3 – Sixteen feasible solutions $\{\mathbf{e}^{(k)}: = (r^{(k)}, g^{(k)}, b^{(k)}); k = 0, 1, \cdots, 15\}$ of the hard shrinkage in the redundant color space.

$\mathbf{e}^{(0)} = (0,0,0)$; $\mathbf{e}^{(1)} = (r_o, g_o, b_o)$
$\mathbf{e}^{(2)} = (t_1, t_1, t_1)$, $t_1 = (r_o + g_o + b_o)/3$
$\mathbf{e}^{(3)} = \left(\frac{2r_o - g_o - b_o}{3}, \frac{-r_o + 2g_o - b_o}{3}, \frac{-r_o - g_o + 2b_o}{3}\right)$
$\mathbf{e}^{(4)} = \left(\frac{2r_o + b_o}{3}, \frac{2g_o + b_o}{3}, \frac{r_o + g_o + b_o}{3}\right)$
$\mathbf{e}^{(5)} = \left(\frac{r_o + g_o + b_o}{3}, \frac{r_o + 2g_o}{3}, \frac{r_o + 2b_o}{3}\right)$
$\mathbf{e}^{(6)} = \left(\frac{2r_o + g_o}{3}, \frac{r_o + g_o + b_o}{3}, \frac{g_o + 2b_o}{3}\right)$
$\mathbf{e}^{(7)} = \left(\frac{2r_o + g_o}{3}, \frac{r_o + 2g_o}{3}, b_o\right)$ $\mathbf{e}^{(8)} = \left(r_o, \frac{2g_o + b_o}{3}, \frac{g_o + 2b_o}{3}\right)$
$\mathbf{e}^{(9)} = \left(\frac{2r_o + b_o}{3}, g_o, \frac{r_o + 2b_o}{3}\right)$
$\mathbf{e}^{(10)} = \left(\frac{r_o - g_o}{3}, \frac{g_o - r_o}{3}, 0\right)$ $\mathbf{e}^{(11)} = \left(0, \frac{g_o - b_o}{3}, \frac{b_o - g_o}{3}\right)$
$\mathbf{e}^{(12)} = \left(\frac{r_o - b_o}{3}, 0, \frac{b_o - r_o}{3}\right)$
$\mathbf{e}^{(13)} = \left(\frac{r_o - b_o}{3}, \frac{g_o - b_o}{3}, \frac{-r_o - g_o + 2b_o}{3}\right)$
$\mathbf{e}^{(14)} = \left(\frac{2r_o - g_o - b_o}{3}, \frac{g_o - r_o}{3}, \frac{b_o - r_o}{3}\right)$
$\mathbf{e}^{(15)} = \left(\frac{r_o - g_o}{3}, \frac{-r_o + 2g_o - b_o}{3}, \frac{b_o - g_o}{3}\right)$

7. APPLICATION TO COLOR IMAGE DENOISING

To remove signal-dependent noise of a color image taken with a certain digital color camera with ISO 1600 sensitivity, the hard color-shrinkage and the hard shrinkage with the redundant color transformation are applied to wavelet coefficients of the three primary color channels. From a standpoint of a balance of simplicity and efficiency, as the wavelet transform, this paper adopts the tight-frame Haar wavelet transform with five multi-resolution layers. In a digital color camera, the variance of signal-dependent noise not only depends on signal intensity, but also differs among the three primary color channels. The signal-dependent noise is well modelled as the following additive noise model [8]:

$$F_{o,p} = S_p + N_p = S_p + w_p(S_p) \cdot N_g, \quad p = R, G, B, \tag{16}$$

$F_{o,p}$: Noisy observation, S_p: Signal, N_p: Signal-dependent noise,
N_g: Gaussian noise with zero mean and unit variance,
w_p: Standard deviation of the noise N_p.

The function w_p defines noise's signal-dependency and determines the standard deviation of noise; it can be measured in advance and utilized for color-image denoising.

In the hard color-shrinkage at each pixel location the three shrinkage parameters, λ_R, λ_G, λ_B, are set so that their values may be inversely proportional to the noise variance:

$$\lambda_p(k) \propto 1/\sigma_{p,n}^2(k), \qquad p = R, G, B, \tag{17}$$

$\sigma_{p,n}(k)$: Standard deviation of noise at a pixel k for the color p.

According to the signal-dependent noise model of (16), $\sigma_{p,n}(k)$ is given by $w_p(S_p)$, but the true noise-free color signal S_p is unknown. To cope with this difficulty, instead of S_p we use scaling coefficients of the noisy input color channels.

The denoising simulations are conducted on noisy test color images, which are produced by adding artificial signal-dependent noise equivalent to ISO 1600 sensitivity to the KODAK standard

color images. Table 4 compares PSNR's [dB] of denoised color images for the color-image set of Fig. 2, among the five different denoising methods: the wavelet denoising with our proposed hard color shrinkage (HCS), the wavelet denoising with our proposed color-shrinkage approach described in Sec. 6 (HS-RCT), the wavelet denoising with the hard shrinkage in the orthogonal opponent color space (HS-OCT), the non-local means method (NLM) [9], and the 3D transform domain collaborative filtering method (CF) [10]. The HS-RCT and the HS-OCT utilize the noise's signal-dependency for denoising in the similar way to the HCS. Our proposed HCS achieves the highest PSNR's, and second to it our proposed HS-RCT shows the highest PSNR's.

Figure 3 shows portions of denoised color images given by the HCS, the HS-RCT and the HS-OCT. The HS-OCT produces false color artifacts as a side effect in the image regions of yellow flowers and bluish metal parts; whereas our proposed methods, the HCS and the HS-RCT, do not produce such false color artifacts, so that they preserve original colors in those image regions more successfully.

8. CONCLUSIONS

As a basic tool for the sparse coding of a color image, we present new hard color-shrinkage that utilizes inter-channel color cross-correlations directly in the primary color space. Moreover, to suppress a false color artifact of the existing shrinkage approach, this paper presents a new simple color-shrinkage approach that applies the classic hard-shrinkage together with a redundant color transformation instead of a usual non-redundant color transformation. This paper applies our two different color-shrinkage schemes to color-image denoising in the tight-frame Haar wavelet transform domain, and experimentally demonstrates that our color-shrinkage schemes suppress false color artifacts more successfully than the existing shrinkage approach.

REFERENCES

[1]S. Mallat, *A wavelet tour of signal processing, 3rd ed.: the sparse way*, Academic Press, 2008.

[2]B. A. Olshausen and D. J. Field, "Sparse coding of sensory inputs," *Curr. Opin. Neurobiol.*, vol.14, pp.481-487, July 2004.

[3]T. Saito and T. Komatsu, "Total-variation approach and wavelet shrinkage for color-image denoising with inter-channel color cross-correlations," in *Proc. IEEE 3rd Int. Symposium on Communication, Control and Signal Processing*, Mar. 2008, pp.494-499.

[4]T. Saito, N. Fujii, and T. Komatsu, "Iterative soft color-shrinkage for color-image denoising," in *Proc. 2009 IEEE Int. Conf. on Image Process.*, Nov. 2009, pp. 3837-3840.

[5]T. Saito, N. Fujii, S. Yoshioka, and T. Komatsu, "Spatially-adaptive wavelet denoising scheme with linear color-shrinkage," in *Proc. EUSIPCO 2008*, Aug. 2008, 1569098800.pdf.

[6]L. Mancera and J. Portilla, "L0-norm-based sparse representation through alternate projections," in *Proc. 2006 IEEE Int. Conf. on Image Process.*, Oct. 2006, pp.2089-2092.

[7]T. Saito and T. Komatsu, "Demosaicing approach based on extended color total-variation regularization," in *Proc. 2008 IEEE Int. Conf. on Image Process.*, Oct. 2008, pp.885-888.

[8]T. Saito, Y. Ishii, R. Nosaka, and T. Komatsu, "Removal of signal-dependent noise for a digital camera," in *Proc. SPIE-IS&T Electronic Imaging, 6502 (Digital Photography III)*, Jan. 2007, pp.6502E:1-6502E:12.

[9]A. Buades, B. Coll, and J. M. Morel, "A review of image denoising algorithms, with a new one," *Multiscale Model. Simul.*, vol.4, no.2, pp.490-530, July 2005.

[10]K. Dabov, A. Foi, V. Katkovnik, and K. Egiazarian, "Image denoising by sparse 3D transform-domain collaborative filtering," *IEEE Trans. Image Process.*, vol.16, no.8, pp.2080-2095, Aug.2007.

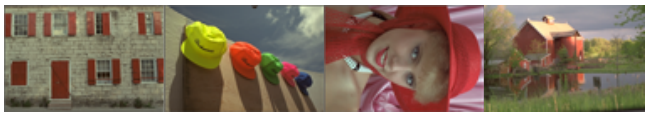

Figure 2 – Set of the original noise-free color images: from the left to the right, No.1, No.2, No.3 and No.4.

Table 4 – Peak SNR's [dB] of denoised images.

	Image No.1	Image No.2	Image No.3	Image No.4
Noisy test color image	21.38	21.08	21.36	21.15
Our new approach: (HCS)	29.20	33.63	31.98	30.56
Our new approach (HS-RCT)	28.97	33.35	31.47	30.31
Existing approach HS-OCT	28.95	33.29	31.34	30.25
NLM [9]	27.14	31.91	30.56	29.37
CF [10]	26.92	32.42	31.08	29.16

(a) Original noise-free image

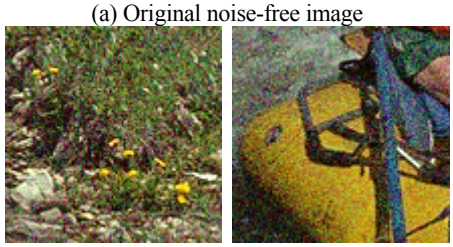

(b) Noisy test color image

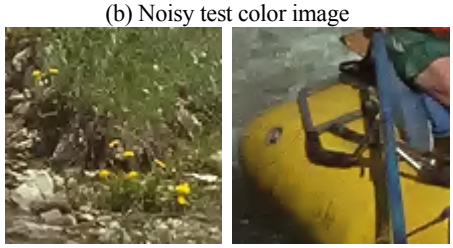

(c) Our proposed HCS

(d) Our proposed HS-RCT

(e) Existing HS-OCT

Figure 3 – Portions of denoised color images.